

Infrared probe of the electronic structure and carrier scattering in NiMnSb thin films

F. B. Mancoff* and B. M. Clemens

Materials Science and Engineering, Stanford University, Stanford, California 94305-2205

E. J. Singley and D. N. Basov

Department of Physics, University of California San Diego, La Jolla, California 92093-0319

(Received 15 July 1999)

We report the use of infrared reflectance spectroscopy to examine the electronic structure of epitaxial, sputter deposited thin films of the predicted half-metallic ferromagnet NiMnSb. The contribution of the interband transitions to the optical conductivity, as well as the spectral weight of conducting carriers, agree with the band structure calculations predicting a half-metallic state in NiMnSb. The intraband response of conducting carriers is different from that of a Drude metal and is consistent with a partial gap in the minority-spin density of states. [S0163-1829(99)51542-7]

Band-structure calculations indicate the ordered compound NiMnSb is a half-metallic ferromagnet, with a metallic majority-spin band and an insulating minority-spin band.^{1,2} Half-metallic electronic structure implies a complete spin polarization of the electronic states at the Fermi energy $P = (N_{\uparrow} - N_{\downarrow}) / (N_{\uparrow} + N_{\downarrow}) = 100\%$, where N_{σ} is the density of states of electrons of spin σ . Half-metallic ferromagnets are of fundamental interest and may be of practical value for magnetic information storage applications, such as giant magnetoresistance spin valves and spin polarized tunnel junctions. Several experimental studies performed on NiMnSb crystals and films have shown properties consistent with the predicted half-metallic structure. The saturation magnetization, necessarily integral for a half metal, was measured as nearly $4\mu_B$ per Mn atom.³ The low-temperature resistivity for NiMnSb does not show the T^2 dependence seen for typical ferromagnets due to spin-flip scattering from magnons, as expected for a half-metallic ferromagnet in which an absence of spin-down states at the Fermi energy prohibits such scattering.^{4,5} Spin-resolved positron annihilation experiments on bulk NiMnSb also indicate a half-metallic state.⁶ However, other direct probes of half-metallic character in NiMnSb have not revealed $P = 100\%$, including spin-polarized photoemission⁷ and superconductor-insulator-ferromagnet tunnel junctions.⁸ Recent superconducting point-contact spectroscopy measurements determined a 50–58% spin polarization.^{9,10} Continued experimental study of the electronic structure in NiMnSb, particularly for thin film samples as required for magnetoelectronic devices, can further examine the possible half-metallic state and its usefulness in applications.

In this paper, we investigate the electronic structure of NiMnSb films using reflectivity measurements over a broad energy range (from the far infrared to the visible). One advantage of this optical experiment is that the bulk of the sample is probed and therefore the data are less affected by any imperfections at the surface. We find that the contribution of interband transitions to the dissipative part of the optical conductivity, as well as the spectral weight associated with the free-carrier absorption, agree with expectations for half-metallic NiMnSb. Moreover, the analysis of the free-

carrier contribution to the complex conductivity suggests a strong frequency dependence of the carrier scattering rate. A characteristic threshold in the scattering rate spectra found at approximately 90 meV can be associated with a lack of spin-flip carrier scattering below this energy and is therefore suggestive of a highly spin polarized electronic structure.

Epitaxial films of NiMnSb on Al_2O_3 (0001) substrates were grown by cosputtering. The preparation and characterization of such NiMnSb films were described previously.^{11,12} For the purpose of the optical measurements, we have prepared films with a thickness of 5000 Å. Using a Drude theory, we found that a 5000 Å film with a dc resistivity below $40\ \mu\Omega\ \text{cm}$ (the typical resistivity of our NiMnSb film at 300 K) shows transmission less than 10^{-4} and therefore can be regarded as being completely opaque within the experimental frequency range $30\text{--}20\,000\ \text{cm}^{-1}$ (4–2500 meV). Symmetric x-ray diffraction shows small amounts ($\sim 1\%$) of additional phases besides NiMnSb present in the film, due to a drift in the sputter sources over the extended deposition time required for the large film thickness. To measure absolute values of $R(\omega)$, we used *in situ* coating of the NiMnSb with gold in the optical cryostat to produce a reference spectrum.¹³ The inset to Fig. 1 shows the NiMnSb reflectance spectra $R(\omega)$ measured at 80 and 300 K in the far-infrared region. $R(\omega)$ decreases with increasing ω at all temperatures, a behavior characteristic of a metal. For temperatures down to 10 K, $R(\omega)$ displayed little temperature dependence, maintaining roughly the same form as the data shown at 80 K. Our results in the visible part of the spectra at 300 K (solid line in Fig. 1) agree well with the ellipsometric data by Kirillova *et al.* (dotted line).¹⁴

Kramers-Kronig (KK) analysis of $R(\omega)$ was used to obtain the complex conductivity $\sigma(\omega) = \sigma_1(\omega) + i\sigma_2(\omega)$. For the analysis, $R(\omega)$ was extrapolated to high energy using the data from Ref. 14. A standard Hagen-Rubens low-energy extrapolation uses the measured dc resistivity in the NiMnSb films ($\rho_{dc} \sim 20$ and $37\ \mu\Omega\ \text{cm}$ for $T = 80$ and 300 K). At low energies [Fig. 2(a)], the coherent response of free carriers leads to a Drude-like peak in $\sigma_1(\omega)$ centered at $\omega = 0$. As the temperature is lowered from 300 to 80 K, the peak narrows and $\sigma_1(\omega \rightarrow 0)$ increases in accord with the dc results

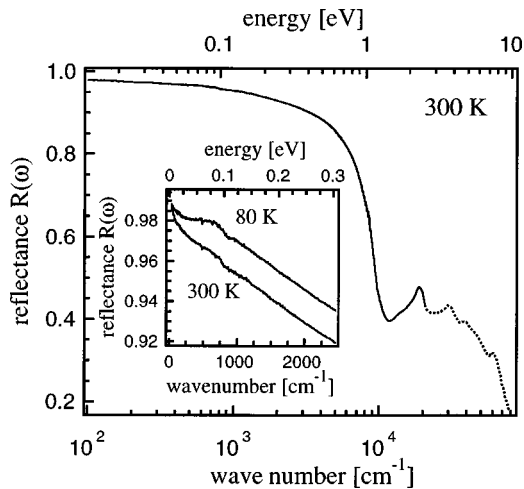


FIG. 1. Reflectance $R(\omega)$ at 300 K (solid line) over extended energy range, including high-energy extrapolation using data from Ref. 14 (dotted line). Inset: The $R(\omega)$ of NiMnSb film at 80 and 300 K decreases with ω in far infrared.

marked by arrows. Figure 2(b) shows the conductivity at 300 K over a broader energy range up to where $\sigma_1(\omega)$ is dominated by interband transitions, including data from the KK analysis (solid line) as well as previous ellipsometry measurements on our NiMnSb films¹¹ (dashed line). The curves

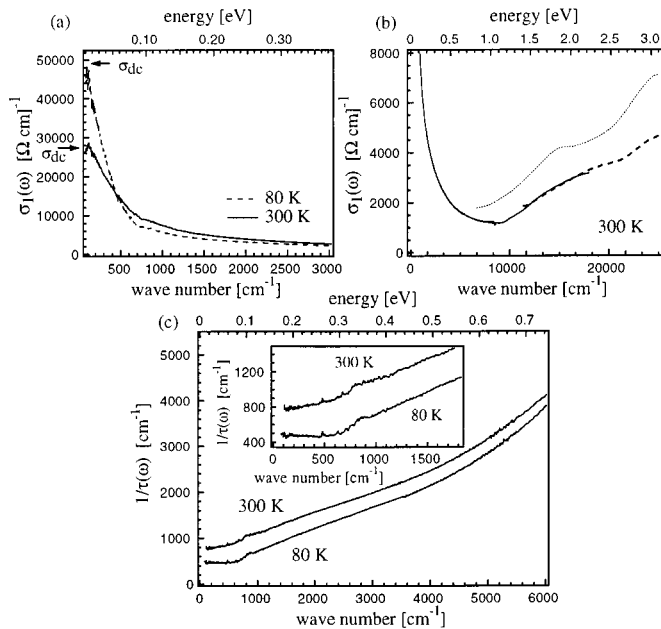


FIG. 2. (a) Frequency dependence of the real part of complex conductivity $\sigma_1(\omega)$ at 80 K (dashed line) and 300 K (solid line) for the intraband region obtained through Kramers-Kronig analysis. The conductivity from standard dc transport measurements, as marked by arrows, is consistent with $\sigma_1(\omega \rightarrow 0)$. (b) $\sigma_1(\omega)$ at 300 K, extended into the interband range (solid line). The dashed line presents previous ellipsometry data for a similar NiMnSb film.¹¹ The dotted line shows theoretical $\sigma_1(\omega)$.¹⁷ (c) The spectra of the scattering rate calculated from conductivity at 80 and 300 K as described in the text. The pronounced frequency dependence of $1/\tau(\omega)$ reveals that the intraband response is different from simple Drude behavior. Inset: Scattering rate curves at low energies show threshold increase at $\sim 700 \text{ cm}^{-1}$ (90 meV) for 80 and 300 K.

from these two experimental techniques are in good agreement in their overlapping energy range. Our data are consistent with previous measurements for other single crystals and films,^{14–16} including both the positive slope of the conductivity spectrum at $\hbar\omega > 1 \text{ eV}$ as well as two shallow peaks at 2.2 and 3 eV. These peaks are also present in the theoretical $\sigma_1(\omega)$ curve (dotted line) that is based on the band-structure calculations suggesting half-metallic ferromagnetism in NiMnSb.¹⁷ The interband features at 2.2 and 3 eV have been associated with electron transitions of the type $p_{\downarrow}(\text{Sb}) \rightarrow d_{\downarrow}(\text{Mn})$ across a minority-spin energy gap at the L and Γ points for the NiMnSb band structure.^{14,16,18}

Attempts to fit the intraband response of $\sigma_1(\omega)$ in Fig. 2(a) using a Drude term $\sigma(\omega) = \sigma_{\text{dc}} / (1 - i\omega\tau)$ show the $\sigma_1(\omega)$ data fall off more slowly than this simple form. To quantify this deviation, we determined the frequency dependence of the scattering rate using the extended Drude model (see Ref. 19 for a review):

$$1/\tau(\omega) = \frac{\omega_p^2}{4\pi} \text{Re} \left(\frac{1}{\sigma(\omega)} \right). \quad (1)$$

The plasma frequency ω_p is calculated from $\omega_p^2 = 8\pi \int_0^{\Omega} \sigma_1(\omega) d\omega$, where the chosen cutoff frequency $\Omega = 8100 \text{ cm}^{-1}$ corresponds to the end of the region dominated by the intraband response, leading to $\omega_p \sim 36000 \text{ cm}^{-1}$ at 300 K, with less than a 1% increase at 80 K. We find that the spectra of $1/\tau(\omega)$ show a pronounced frequency dependence [Fig. 2(c)]. Except for the lowest frequencies, the absolute value of the scattering rate is smaller than ω , which is in accord with the Fermi-liquid theory. Notably, $1/\tau(\omega)$ reveals nearly linear ω dependence between 1000 and 4500 cm^{-1} which is in disagreement with the ω^2 behavior expected in a metal.²⁰ The scattering rate spectra at 80 and 300 K show a kink at 700 cm^{-1} (90 meV), with $1/\tau(\omega)$ at 80 K remaining nearly flat up to this threshold ω [inset to Fig. 2(c)]. As will be discussed, the unusual quasilinear increase in $1/\tau(\omega)$ as well as the kink can be attributed to a peculiar electronic structure of NiMnSb. Also, $1/\tau(\omega)$ in the limit of $\omega \rightarrow 0$ decreases with lower temperature, consistent with the dc transport.

A threshold structure in the $1/\tau(\omega)$ spectrum of a conducting material is suggestive of an abrupt increase of scattering. For a ferromagnetic metal such as NiMnSb, such an increase can be attributed to the energy difference Δ between the Fermi energy E_F and the onset of the conduction band for the spin-down electrons. In a half-metallic ferromagnet at low temperatures and $\hbar\omega < \Delta$ [$\sim 700 \text{ cm}^{-1}$ or 90 meV for NiMnSb as determined in Fig. 2(c)], spin-flip scattering is forbidden due to the lack of available spin-down states at that energy. These spin-flip events may result from scattering by magnons or other magnetic impurities, such as local deviations in magnetic ordering due to atomic site disorder or nonstoichiometry in the NiMnSb compound. Note that the threshold in $1/\tau(\omega)$ also persists in the 300 K spectrum, as can be expected for a ferromagnet with a Curie temperature above room temperature. Recent experimental study of CrO_2 , another half-metallic ferromagnet,²¹ also observed such a threshold increase in $1/\tau(\omega)$.²²

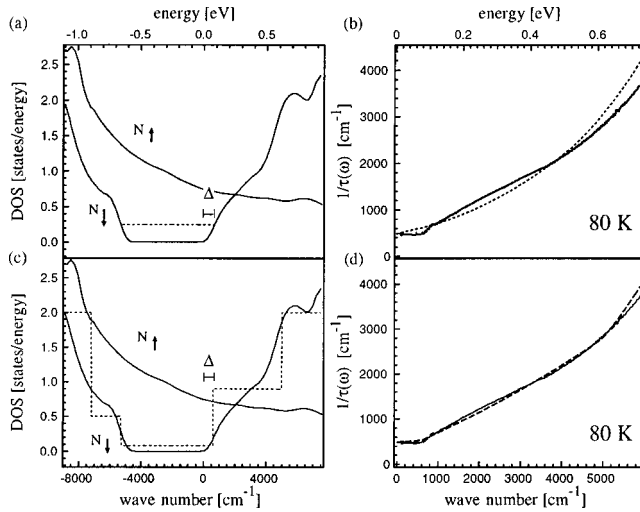


FIG. 3. (a) Spin-dependent density of states (DOS) $N_{\uparrow}(\omega)$ and $N_{\downarrow}(\omega)$ (solid lines) are taken from Ref. 2. The position of $N_{\downarrow}(\omega)$ has been shifted down in ω by 1470 cm^{-1} (0.18 eV) to reproduce the frequency location of the observed scattering rate threshold structure at $\sim 700 \text{ cm}^{-1}$ (90 meV). The pseudogap in $N_{\downarrow}(\omega)$ (dashed line) is set to produce the 50% spin polarization at the Fermi level from the Andreev reflection suppression data (Ref. 10). (b) The frequency dependence of scattering rate at 80 K (solid line). The dashed line shows the result of spin-flip scattering rate simulation using Eq. 2 with $N_{\uparrow}(\omega)$ and $N_{\downarrow}(\omega)$ with pseudogap from (a). (c) The smooth features in $N_{\downarrow}(\omega)$ were approximated with rectangular steps (dashed line). The lowered pseudogap gives enhanced spin polarization $P > 50\%$ resulting from setting $v_F^{\downarrow}/v_F^{\uparrow} = 3$ for scattering rate simulation. (d) The scattering rate data (solid line) and simulation (dashed line) using $N_{\uparrow}(\omega)$ and rectangular steps for $N_{\downarrow}(\omega)$ from (c).

In Fig. 3, we simulate the behavior of $1/\tau(\omega)$ using a model proposed in Ref. 23 suggesting that spin-flip scattering processes lead to the following frequency dependence of the scattering rate:

$$1/\tau_{sf}(\omega) \propto \int_{-\omega/2}^{\omega/2} [N_{\downarrow}(\omega' - \omega/2)N_{\uparrow}(\omega' + \omega/2) + N_{\downarrow}(\omega' + \omega/2)N_{\uparrow}(\omega' - \omega/2)] d\omega'. \quad (2)$$

In Eq. 2, $N_{\uparrow}(\omega)$ and $N_{\downarrow}(\omega)$ denote the density of states (DOS) for the majority and minority spins, respectively. As expected, the model yields $1/\tau_{sf}(\omega) = 0$ for $\hbar\omega < \Delta$ in a half metal. In Eq. 2, we use $N_{\uparrow}(\omega)$ and $N_{\downarrow}(\omega)$ for NiMnSb from the theoretical calculations of Ref. 2 [solid lines in Figs. 3(a) and (c)], with two modifications. First, the complete energy gap, for which $N_{\downarrow}(\omega) = 0$ around E_F as calculated, is replaced with a pseudogap [dashed line in Fig. 3(a)], introducing a constant, nonzero $N_{\downarrow}(\omega)$ over the gap range. This pseudogap reduces the spin polarization at E_F from the half metallic $P = 100\%$ down to $\sim 50\%$ in accord with recent Andreev reflection measurements with a superconducting point contact.^{10,24} Such a suppression of the spin polarization may result from atomic disorder or defects in the NiMnSb lattice.²⁵ As a second modification to the theoretical DOS, we shift $N_{\downarrow}(\omega)$ in energy with respect to $N_{\uparrow}(\omega)$ and the Fermi level $\omega = 0$. The chosen extent of the shift adjusts the position of E_F within the pseudogap in $N_{\downarrow}(\omega)$ so as to re-

produce correctly the frequency location of the threshold feature in the $1/\tau(\omega)$ data. Following this shift, E_F still remains closer to the minority-spin conduction band than to the valence band, as theoretically calculated.² Finally, the scattering rate simulations also include a proportionality factor and a constant offset added to Eq. 2.

The simulated $1/\tau(\omega)$ from Eq. 2 using the modified $N_{\uparrow}(\omega)$ and $N_{\downarrow}(\omega)$ from Fig. 3(a) is shown with the dashed line in Fig. 3(b). The simulation reproduces the general shape of the 80 K experimental $1/\tau(\omega)$ (solid line). However, the experimental scattering rate is nearly flat for ω below the threshold, as expected for a $P = 100\%$ half-metallic ferromagnet with $\hbar\omega < \Delta$, and increases sharply above the threshold. The simulated $1/\tau(\omega)$, though, shows a slight positive slope for low ω , since the pseudogap used for $N_{\downarrow}(\omega)$ gives $P = 50\%$, which allows limited spin-flip scattering even below Δ . Since reproduction of the flat region in $1/\tau(\omega)$ at low ω using Eq. 2 requires a complete spin polarization, we examine possible explanations for this discrepancy in the suppressed slope of $1/\tau(\omega)$. We note that the electronic structure shown in Fig. 3 will also lead to suppression of nonmagnetic scattering due to the lack of final states for $\hbar\omega < \Delta$. Equation 2 does not account for these processes, though. Also, the Andreev reflection technique may yield a polarization $P_c \sim 50\%$ that is artificially lowered due to local disruption of the ideal $C1_b$ NiMnSb unit cell by damage from insertion of the superconducting point contact tip. Finally, due to the different definitions of P and P_c ,^{24,26} a Fermi velocity ratio $v_F^{\downarrow}/v_F^{\uparrow} > 1$ would give $P > P_c = 50\%$, thus producing a lower $N_{\downarrow}(\omega)$ pseudogap level and a flatter simulated $1/\tau(\omega)$ below the frequency threshold. An improved correspondence with the curvature of the $1/\tau(\omega)$ data over the range up to $\omega \sim 6000 \text{ cm}^{-1}$ is obtained using an approximation of the features in $N_{\downarrow}(\omega)$ with rectangular steps [dashed line in Fig. 3(c)]. For this $N_{\downarrow}(\omega)$, we also include a pseudogap which has a relatively low level determined by using $P_c = 50\%$ and setting $v_F^{\downarrow}/v_F^{\uparrow} = 3$. The resulting $1/\tau(\omega)$ simulation [dashed line in Fig. 3(d)] almost completely reproduces the experimental spectrum, including a highly suppressed slope at low ω as a result of an enhanced P due to the lowered pseudogap level. A similar simulation using the rectangular steps for $N_{\downarrow}(\omega)$ but with the pseudogap level set by $v_F^{\downarrow}/v_F^{\uparrow} = 1$ and $P = P_c = 50\%$ also agrees with the $1/\tau(\omega)$ data at high ω but contains a noticeably greater slope of $1/\tau(\omega)$ below the threshold than observed. Finally, as a comparison with the NiMnSb data, we are not aware of any previous experimental $1/\tau(\omega)$ analysis for an elemental ferromagnet with $P < 100\%$. However, we have used Eq. 2 and the theoretical $N_{\uparrow}(\omega)$ and $N_{\downarrow}(\omega)$ for ferromagnetic Fe (Ref. 27) to produce a simulated $1/\tau(\omega)$ spectrum, which as expected does not show any threshold for suppression of $1/\tau(\omega)$ at low ω .

We also discuss the carrier density n in NiMnSb in conjunction with our result for the plasma frequency $\omega_p^2 = 4\pi n e^2/m^*$, where m^* is the effective mass of conducting carriers and e is the electron charge. Our result for $\omega_p = 36000 \text{ cm}^{-1}$ includes approximately a 10–15% uncertainty in the value of the n/m^* ratio. This uncertainty is related to the somewhat ambiguous choice of the cutoff frequency $\Omega = 8100 \text{ cm}^{-1}$ in the integral of the conductivity $\sigma_1(\omega)$. Contributions to this integral due to interband tran-

sitions that extend below the cutoff Ω are calculated and removed using a description of the interband conductivity in terms of Lorentz oscillators,¹⁶ giving a decrease for ω_p of $\sim 2\%$. Assuming the free-electron mass for m^* , the ω_p value corresponds to $n \sim 0.7$ conducting carriers per NiMnSb formula unit. This estimate is in reasonable agreement with band-structure calculations that suggest the conducting states are holes in a partially occupied Sb $5p$ band,¹ with an expected concentration of one hole per NiMnSb formula unit for the half-metallic state.⁴

In summary, we investigated the electronic structure of thin films of the predicted half-metallic ferromagnet NiMnSb using optical reflectance spectroscopy. For energies in the region of interband transitions, the optical conductivity agrees with results for bulk NiMnSb understood in terms of the theoretical half-metallic band structure. The frequency

dependent carrier scattering rate indicates a deviation from ideal Drude behavior in the intraband region. The scattering rate increases sharply above a threshold frequency, suggesting the onset of an additional scattering channel which can be connected to spin-flip processes. A model to describe the experimental scattering rate spectrum uses a realistic spin-dependent density of states. Therefore, both interband and intraband contributions to the optical conductivity are indicative of an electronic structure for NiMnSb with a high degree of spin polarization.

Financial support from the NSF through the Stanford Center for Materials Research MRSEC and the Fannie and John Hertz Foundation (F.B.M.) is acknowledged. Work at UCSD was supported through the NSF Grant No. DMR-9875980. D.N.B. received funding from the Research Corporation.

*Author to whom correspondence should be addressed. Electronic address: fred.mancoff@stanford.edu

¹R. A. de Groot, F. M. Mueller, P. G. van Engen, and K. H. J. Buschow, Phys. Rev. Lett. **50**, 2024 (1983).

²S. J. Youn and B. I. Min, Phys. Rev. B **51**, 10 436 (1995).

³R. B. Helmholdt, R. A. de Groot, F. M. Mueller, P. G. van Engen, and K. H. J. Buschow, J. Magn. Magn. Mater. **43**, 249 (1984).

⁴M. J. Otto, R. A. M. van Woerden, P. J. van der Valk, J. Wijngaard, C. F. van Bruggen, and C. Haas, J. Phys.: Condens. Matter **1**, 2351 (1989).

⁵J. S. Moodera and D. M. Mootoo, J. Appl. Phys. **76**, 6101 (1994).

⁶K. E. H. M. Hanssen, P. E. Mijnaerends, L. P. L. M. Rabou, and K. H. J. Buschow, Phys. Rev. B **42**, 1533 (1990).

⁷G. L. Bona, F. Meier, M. Taborelli, E. Bucher, and P. H. Schmidt, Solid State Commun. **56**, 391 (1985).

⁸R. Kabani, M. Terada, A. Roshko, and J. S. Moodera, J. Appl. Phys. **67**, 4898 (1990).

⁹R. J. Soulen, Jr., J. M. Byers, M. S. Osofsky, B. Nadgorny, T. Ambrose, S. F. Cheng, P. R. Broussard, C. T. Tanaka, J. Nowak, J. S. Moodera, A. Barry, and J. M. D. Coey, Science **282**, 85 (1998).

¹⁰F. B. Mancoff, B. M. Clemens, B. Nadgorny, M. S. Osofsky, and R. J. Soulen, Jr. (unpublished).

¹¹J. F. Bobo, P. R. Johnson, M. Kautzky, F. B. Mancoff, E. Tuncel, R. L. White, and B. M. Clemens, J. Appl. Phys. **81**, 4164 (1997).

¹²F. B. Mancoff, M. C. Kautzky, J. F. Bobo, O. E. Richter, R. Sinclair, and B. M. Clemens (unpublished).

¹³C. C. Homes, M. Reedyk, D. A. Cradles, and T. Timusk, Appl. Opt. **32**, 2976 (1993).

¹⁴M. M. Kirillova, A. A. Makhnev, E. I. Shreder, V. P. Dyakina, and N. B. Gorina, Phys. Status Solidi B **187**, 231 (1995).

¹⁵P. A. M. van der Heide, W. Baelde, R. A. de Groot, A. R. de Vroomen, P. G. van Engen, and K. H. J. Buschow, J. Phys. F **15**, L75 (1985).

¹⁶X. Gao, J. Woollam, R. D. Kirby, D. J. Sellmyer, C. T. Tanaka, J. Nowak, and J. S. Moodera, Phys. Rev. B **59**, 9965 (1999).

¹⁷V. N. Antonov, P. M. Oppeneer, A. N. Yaresko, A. Ya. Perlov, and T. Kraft, Phys. Rev. B **56**, 13 012 (1997).

¹⁸S. V. Halilov and E. T. Kulatov, J. Phys.: Condens. Matter **3**, 6363 (1991).

¹⁹A. V. Puchkov, D. N. Basov, and T. Timusk, J. Phys.: Condens. Matter **8**, 10 049 (1996).

²⁰D. Pines and P. Nozieres, *The Theory of Quantum Liquids* (W. A. Benjamin, New York, 1966).

²¹K. Schwarz, J. Phys. F **16**, L211 (1986).

²²E. J. Singley, D. N. Basov, C. P. Weber, A. Barry, and J. M. D. Coey, Phys. Rev. B **60**, 4126 (1999).

²³I. I. Mazin, D. J. Singh, and C. Ambrosch-Draxl, Phys. Rev. B **59**, 411 (1999).

²⁴The point-contact spectroscopy technique actually measures, in the limit of ballistic transport, a spin polarization at E_F given by $P_c = (N_\uparrow v_F^\uparrow - N_\downarrow v_F^\downarrow) / (N_\uparrow v_F^\uparrow + N_\downarrow v_F^\downarrow)$, which is weighted by the relative Fermi velocities v_F for spin-up and spin-down electrons as opposed to the unweighted P relevant to the present analysis. The level of the pseudogap in N_\downarrow [dashed line in inset to Fig. 3(a)] is set to give simply $P = 50\%$ at E_F , neglecting the Fermi velocity weighting for now.

²⁵D. Orgassa, H. Fujiwara, T. C. Schulthess, and W. H. Butler, Phys. Rev. B (to be published).

²⁶I. I. Mazin, Phys. Rev. Lett. **83**, 1427 (1999).

²⁷R. A. Tawil and J. Callaway, Phys. Rev. B **7**, 4242 (1973).